Int. J. Heat Mass Transfer. Vol. 29, No. 12, pp. 1869–1880, 1986
Printed in Great Britain

0017–9310/86 $3.00 + 0.00
Pergamon Journals Ltd.

Analytical and experimental investigation of simultaneous melting–condensation on a vertical wall in the presence of a noncondensable gas

D. GALAMBA, V. K. DHIR* and KAVEH TAGHAVI†

School of Engineering and Applied Science, University of California—Los Angeles, Los Angeles, CA 90024, U.S.A.

(*Received* 19 *August* 1985 *and in final form* 12 *March* 1986)

Abstract—Simultaneous melting–condensation on a vertical wall with noncondensable gas in the vapor is investigated analytically and experimentally. Using similarity transformations, the full boundary-layer equations governing the immiscible melt, the condensate and the vapor–gas layers are solved numerically. Results are obtained for the melting heat transfer rate both without and with noncondensables and interfacial resistance. In the analysis low and high Prandtl number melts are considered while the condensate is assumed to be a high Prandtl number liquid. Experiments are conducted by condensing steam with air onto vertical surfaces of naphthalene and Wood's metal slabs. The data are found to compare well with the no interfacial resistance and large condensation coefficient predictions.

INTRODUCTION

WHEN a solid structure is exposed to a vapor–noncondensable gas mixture and the melting temperature of the solid is less than the temperature of the mixture, simultaneous melting–condensation may occur. This phenomenon is of particular interest in nuclear reactor safety and has several applications in the chemical industry such as desalination. In this work, steady-state condensation–melting of a vertical surface exposed to vapor of another liquid with noncondensable gas in it is studied.

The problems of steady-state condensation and steady-state condensation–melting for vertical surfaces in the absence of a noncondensable gas have been studied by several investigators including Taghavi-Tafreshi and Dhir [1]. In ref. [1] steady-state simultaneous melting–condensation on a vertical wall with no noncondensable gas in the vapor was investigated both analytically and experimentally. Using similarity transformations, the full constant property boundary-layer equations governing the laminar melt and condensate films were solved numerically for high Prandtl number liquids. In ref. [2] Taghavi-Tafreshi extended these results to relax the high Prandtl number restriction. Both the inertia terms in the momentum equations and the convective terms in the energy equations were included in this later work.

The problems of steady-state condensation and steady-state condensation–melting with a noncondensable gas present in the vapor have been studied by several investigators including Sparrow and Lin [3], Minkowycz and Sparrow [4] and Yen *et al.* [5]. In ref. [3] Sparrow and Lin investigated the problem of condensation onto a vertical wall with a noncondensable gas in the vapor. The molecular weight of the gas was assumed to be higher than that of the vapor. For the condensate layer, they assumed a constant property Nusselt-type analysis. Constant properties were also assumed for the vapor–gas mixture. The buoyancy term in the mixture momentum equation was modeled using the ideal gas law and it was assumed that the temperature variations across the mixture layer were insignificant. The governing boundary-layer equations for the mixture layer were transformed into ordinary differential equations using similarity transformations. The differential equations were then formally integrated and numerically solved by iteration of trial solutions. Results were presented for the steam–air system. They then compared their analytical results with the experimental results of Othmer [6] and found that the agreement between the two was quite satisfactory. Minkowycz and Sparrow [4] refined the analysis presented in ref. [3]. In this later work variable fluid properties were taken into account in both the mixture and the liquid layers. The buoyancy term in the momentum equation considered both concentration and temperature variations. The governing partial differential equations were transformed into similar form and were then formally integrated and solved numerically by iteration. Results were once again presented for the steam–air system. These refined analytical results were then compared with those presented in ref. [3] and the agreement between the two was satisfactory. Yen *et al.* [5] investigated both analytically and experimentally steam with air in it condensing onto a vertical slab of ice. The authors used the work of Tien and Yen [7] to analyze the constant property condensate–melt layer

* To whom correspondence should be addressed.
† Presently at University of Kentucky, Lexington, KY 40506, U.S.A.

NOMENCLATURE

a	condensation coefficient
c	constant defined in equations (11), (17) and (25)
c_p	specific heat
D	diffusion coefficient
$F, \tilde{F}$	similarity function
f	similarity function for the vapor–gas mixture
g	gravity
$\bar{h}$	average heat transfer coefficient
h_{fg}	latent heat of vaporization of the condensate
h_{sl}	latent heat of fusion of the solid
h'_{sl}	h_{sl} corrected for subcooling of the solid
k	thermal conductivity
L	surface height
M	$M_g/(M_g - M_v)$
M_g	molecular weight of the gas
M_v	molecular weight of the vapor
m_g	mass fraction of the gas
Nu	Nusselt number
Pr	Prandtl number
Q	rate of heat transfer
q	heat flux at wall with gas in vapor
q_0	heat flux at wall with no gas in vapor and no interfacial resistance
R	thermal resistance
R_v	gas constant of the vapor
$R_2, R_3, R_4, R_5, R_6, R_7$	constants defined in equations (35), (36), (37), (38), (40) and (45)
Sc	Schmidt number
T	temperature [K]
T_{melt}	melting temperature of the solid
T_{sat}	saturation temperature of the vapor
T_0	subcooled temperature of the solid
u	component of velocity in the x-direction
v	component of velocity in the y-direction
W	surface width
x	axial coordinate parallel to gravitational acceleration and measured from leading edge of the solid wall
y	coordinate normal to the surface.

Greek symbols

α	thermal diffusivity
γ	coefficient in the expression for the Nusselt number
Δm	net melted mass lost during an experiment
Δp	vapor pressure drop at the free surface
Δt	duration of the experiment
δ	film thickness
ε	T/T_∞
$\eta, \tilde{\eta}$	similarity variable defined in equations (10), (16) and (24)
η_{max}	maximum η considered in the vapor–gas mixture layer
$\theta, \tilde{\theta}$	dimensionless film temperature defined in equations (12) and (18)
μ	viscosity
ν	kinematic viscosity
ρ	density
ϕ	$m_g - m_{g\infty}$
ψ	stream function.

Subscripts

no subscript	vapor–gas mixture layer
c	condensate layer
f	refers to the free surface at $y = \delta_m + \delta_c$
i	refers to interface between the condensate and melt layers
m	melt layer
s	solid
t	total or overall
x	derivative with respect to x
y	derivative with respect to y
∞	refers to value in the vapor–gas bulk far away from the free surface.

Superscripts

$'$	derivative of the function with respect to its argument
0	evaluated at inner edge of the layer
1	evaluated at outer edge of the layer
-	averaged over the height of the melting surface.

and that of Sparrow and Lin [3] to analyze the steam–air mixture layer. The similarity equations for the vapor–gas layer were formally integrated and solved iteratively. Experiments were conducted with a mass fraction of the air in the steam ranging from 0.12 to 0.59. The analytical and experimental results were found to be in good agreement.

In this work condensation-driven melting of a vertical wall is analyzed for the case when the melt and the condensate are two different immiscible substances and a noncondensable gas is present in the vapor. The constant property governing equations for the condensate and melt layers are formulated the same way as was done in ref. [2] while those for the vapor–gas mixture are set up as was done in ref. [3] but including the temperature variation in the buoyancy term of the momentum equation [5]. The inertia and convective terms are retained in the condensate and melt momentum and energy equations. Unlike the approach taken in refs. [3–5] the governing equations are not formally integrated and solved by iteration of trial solutions; rather they are numerically integrated

in their differential form using a higher-order accurate Runge–Kutta routine and a predictor-and-corrector method. Experiments were conducted by condensing steam with air in it on the vertical faces of slabs made of naphthalene and Wood's metal. The Prandtl numbers of the naphthalene and Wood's metal melt layers are 10.0 and 0.0251, respectively. These two materials thus represent the usually called 'large and small Prandtl number limits'.

ANALYSIS

The physical model used in this study is shown in Fig. 1. A vertical, isothermal wall at its melting temperature is exposed to a vapor of another immiscible liquid with a noncondensable gas present in the vapor. The melting temperature of the wall is less than the bulk temperature of the vapor–gas mixture which is also at least the saturation temperature corresponding to the partial pressure of the vapor. The latent heat of vaporization released during condensation of the vapor leads to melting of the solid. The vapor condenses in the form of a film and both the melt and condensate films flow downwards due to gravity. The various assumptions made are:

1. During the melting process, which is assumed to be steady, the wall is maintained at its melting temperature. The analysis will be valid for subcooled walls for times greater than $[25\pi c_{ps}k_s\rho_s(T_{melt}-T_0)^2/q^2]$ provided the latent heat of fusion is corrected to account for subcooling of the wall by

$$h'_{sl} = h_{sl} + c_{ps}(T_{melt} - T_0). \tag{1}$$

The above steady-state time criterion was obtained using results presented in ref. [8].

2. The condensate spreads very easily on the melt layer so that filmwise rather than dropwise condensation occurs.

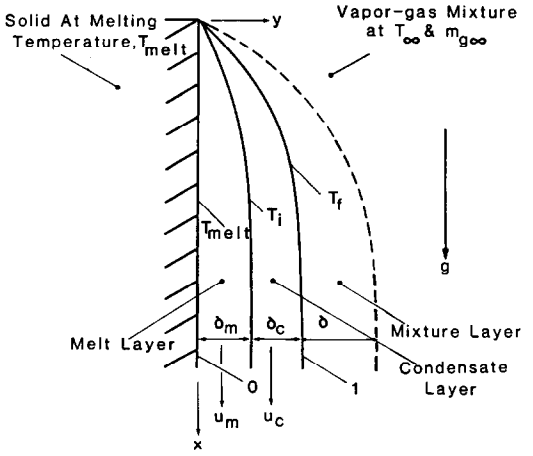

FIG. 1. Physical model for simultaneous melting–condensation on a vertical wall with noncondensable gas in the vapor.

3. The transient times during which the condensate and melt layers reach their steady-state thicknesses are much smaller than the times of interest. This can be confirmed using the analysis presented in ref. [9].

4. The leading edge region where surface tension between the two liquids could be important is much smaller than the height of the melting surface.

5. In the assumed two-film model, the melting rate will be a function of x, and because of this the initially vertical wall will start to deviate from its original shape. In the present work the surface is assumed to remain vertical. Therefore, the present analysis is valid only for time periods in which the deviation of the melting surface from the original vertical shape is small.

6. The axes are fixed on the wall and move into the solid as the melting front progresses. Thus each new position of the axes represents a quasi-static state.

7. The molecular weight of the noncondensable gas is greater than that of the vapor.

8. Constant properties are assumed for both the condensate and melt layers as well as for the vapor–gas mixture. The analysis will be presented for the case of the condensate Prandtl number being greater than one and the melt Prandtl number being less than one. However, with minor analytical changes which are presented in ref. [2] any Prandtl number combination of condensate and melt can be treated.

Evidently, assumptions 3 and 5 can be conflicting; but the times at which a significant change in the shape occurs will generally be at least an order of magnitude longer than the times at which the melt and condensate layers reach their steady-state thicknesses. This will be discussed later.

The steady-state, constant property, boundary-layer equations for either the melt, condensate, or the vapor–gas mixture layers are

$$u_{jx} + v_{jy} = 0 \tag{2}$$

$$u_j u_{jx} + v_j u_{jy} = g(\rho_j - \rho_\infty)/\rho_j + \nu_j u_{jyy} \tag{3}$$

$$u_j T_{jx} + v_j T_{jy} = \alpha_j T_{jyy} \tag{4}$$

where the subscript j refers to either the melt, condensate, or the vapor–gas mixture layers. In the following analysis the melt layer is denoted by the subscript m, the condensate layer by the subscript c, and the vapor–gas mixture has no subscript. Furthermore for the vapor–gas mixture the species equation is

$$u m_{gx} + v m_{gy} = D m_{gyy}. \tag{5}$$

The following boundary and interface conditions are applicable to the layers

$$u_m = 0, \quad T_m = T_{melt} \quad \text{at } y = 0 \tag{6}$$

$$\left.\begin{aligned} &u_m = u_c, \quad v_m = v_c, \quad T_m = T_i, \quad T_c = T_i, \\ &\mu_m \partial u_m/\partial y = \mu_c \partial u_c/\partial y, \\ &v_m/u_m = \mathrm{d}\delta_m/\mathrm{d}x \end{aligned}\right\} \text{at } y = \delta_m \tag{7}$$

$$\left.\begin{aligned} &u = u_c,\\ &\rho[u\mathrm{d}(\delta_m+\delta_c)/\mathrm{d}x - v] = \rho_c[u_c\mathrm{d}(\delta_m+\delta_c)/\mathrm{d}x - v_c],\\ &\mu_c\partial u_c/\partial y = \mu\partial u/\partial y, \quad T_c = T_f, \quad T = T_f,\\ &\rho u m_g\mathrm{d}(\delta_m+\delta_c)/\mathrm{d}x + \rho D\partial m_g/\partial y - m_g\rho v = 0,\\ &m_g = m_{gf} \end{aligned}\right\}$$

$$\text{at } y = \delta_m+\delta_c \quad (8)$$

$$u = 0, \quad T = T_\infty, \quad m_g = m_{g\infty} \qquad \text{at } y = \infty. \quad (9)$$

The last interface condition in equation (7) results from the fact that a fluid particle at the melt–condensate interface should follow the interface path line since there is no mass transfer across that interface. The second interface condition in equation (8) is mass continuity at the free surface. The next to last condition in equation (8) is due to the fact that at the free surface, air is insoluble in the condensate layer. The interfacial and boundary conditions listed above do not include the matching of the heat fluxes at the melt–condensate interface. This condition will be used later to determine the temperature of this interface.

For a low Prandtl number melt layer, a similarity parameter $\tilde{\eta}_m$ for the melt layer is defined as

$$\tilde{\eta}_m = Pr_m^{-1/4}c_m y/x^{1/4} \quad (10)$$

where

$$c_m = [gc_{pm}(\rho_m-\rho_\infty)/(4\nu_m k_m)]^{1/4}. \quad (11)$$

The similarity functions are defined as

$$\left.\begin{aligned} &\tilde{F}_m(\tilde{\eta}_m) = Pr_m^{-3/4}\psi_m/(4\alpha_m c_m x^{3/4}),\\ &\tilde{\theta}_m(\tilde{\eta}_m) = (T_m - T_{melt})/(T_i - T_{melt}). \end{aligned}\right\} \quad (12)$$

In equation (12) ψ_m is the stream function for the melt layer. The melt velocities are related to the similarity function $\tilde{F}_m$ as

$$\left.\begin{aligned} &u_m = 4\alpha_m c_m^2 Pr_m^{1/2}x^{1/2}\tilde{F}'_m,\\ &v_m = \alpha_m c_m Pr_m^{3/4}x^{-1/4}[\tilde{\eta}_m\tilde{F}'_m - 3\tilde{F}_m]. \end{aligned}\right\} \quad (13)$$

Using the transformations (10)–(13), the momentum and energy equations for the melt layer become

$$\tilde{F}'''_m + 3\tilde{F}_m\tilde{F}''_m - 2(\tilde{F}'_m)^2 + 1 = 0 \quad (14)$$

$$\tilde{\theta}''_m + 3Pr_m\tilde{F}_m\tilde{\theta}'_m = 0. \quad (15)$$

For a high Prandtl number condensate layer the similarity variable and functions are given in ref. [1]

$$\eta_c = c_c(y-\delta_m)/x^{1/4} \quad (16)$$

where

$$c_c = [gc_{pc}(\rho_c-\rho_\infty)/(4\nu_c k_c)]^{1/4} \quad (17)$$

$$F_c(\eta_c) = \psi_c/(4\alpha_c c_c x^{3/4}),$$

$$\theta_c(\eta_c) = (T_c - T_i)/(T_f - T_i). \quad (18)$$

The condensate velocities are

$$\left.\begin{aligned} &u_c = 4\alpha_c c_c^2 x^{1/2}F'_c,\\ &v_c = \alpha_c c_c x^{-1/4}[(\eta_c + (c_c/c_m)\eta_{\delta m})F'_c - 3F_c]. \end{aligned}\right\} \quad (19)$$

Using the transformations (16)–(19) the governing equations for the condensate layer become

$$F'''_c + (1/Pr_c)[3F_cF''_c - 2(F'_c)^2] + 1 = 0 \quad (20)$$

$$\theta''_c + 3F_c\theta'_c = 0. \quad (21)$$

As was done in refs. [3, 5] the difference in densities in the buoyancy term of the vapor–gas mixture momentum equation is given by

$$(\rho-\rho_\infty)/\rho = [(M-m_{g\infty})(1-\varepsilon)+\varepsilon\phi]/[M-m_{g\infty}] \quad (22)$$

where

$$M = M_g/(M_g - M_v), \quad \varepsilon = T/T_\infty, \quad \phi = m_g - m_{g\infty}. \quad (23)$$

Using the similarity variable and functions given in ref. [3]

$$\eta = c[y-(\delta_m+\delta_c)]/x^{1/4} \quad (24)$$

where

$$c = \{g/[4\nu^2(M-m_{g\infty})]\}^{1/4} \quad (25)$$

$$f(\eta) = \psi/(4\nu c x^{3/4}), \quad \varepsilon(\eta) = T/T_\infty,$$

$$\phi(\eta) = m_g - m_{g\infty}. \quad (26)$$

The vapor–gas mixture velocities are

$$u = 4\nu c^2 x^{1/2}f', \quad v = \nu c x^{-1/4}\{[\eta + (c/c_c)\eta_{\delta c}]f' - 3f\}. \quad (27)$$

With the transformations (24)–(27) the vapor–gas momentum, energy and species equations become

$$f''' + 3ff'' - 2(f')^2 + \phi\varepsilon + (1-\varepsilon)(M-m_{g\infty}) = 0 \quad (28)$$

$$\varepsilon'' + 3Prf\varepsilon' = 0 \quad (29)$$

$$\phi'' + 3Scf\phi' = 0. \quad (30)$$

The boundary and interface conditions are transformed as

$$\tilde{F}'_m = 0, \quad \tilde{\theta}_m = 0 \qquad \text{at } \tilde{\eta}_m = 0 \quad (31)$$

$$\left.\begin{aligned} &\tilde{F}'_m = Pr_c^{-1/2}F'_c, \quad F_c = 0, \quad \theta_m = 1, \quad \theta_c = 0\\ &\qquad\qquad \text{at } \tilde{\eta}_m = \tilde{\eta}_{\delta m}\\ &\tilde{F}''_m = Pr_m^{-1/4}R_2F''_c, \quad \tilde{F}_m = 0 \quad \text{or } \eta_c = 0 \end{aligned}\right\}$$

(32)

$$\left.\begin{aligned} &f' = R_4 F_c', \quad f = R_5 F_c, \quad F_c'' = R_6 f'', \quad \text{at } \eta_c = \eta_{\delta c} \\ &\theta_c = 1, \quad \varepsilon = T_f/T_\infty, \\ &\quad \phi'(0)/[\phi(0)+m_{g\infty}]+3Scf(0) = 0, \\ &\phi(0) = m_{gf}-m_{g\infty} \qquad \text{or } \eta = 0 \end{aligned}\right\} \tag{33}$$

$$f' = 0, \quad \varepsilon = 1, \quad \phi = 0 \qquad \text{at } \eta = \infty \tag{34}$$

where

$$R_2 = \mu_c \alpha_c c_c^3/(\mu_m \alpha_m c_m^3) \tag{35}$$

$$R_4 = [(M-m_{g\infty})/Pr_c]^{1/2} \tag{36}$$

$$R_5 = \rho_c \alpha_c c_c/(\rho v c) \tag{37}$$

$$R_6 = \mu v c^3/(\mu_c \alpha_c c_c^3). \tag{38}$$

Another interface condition is that at the free surface a saturation state exists for the condensing vapor. There are three other parameters: T_i, $\tilde{\eta}_{\delta m}$ and $\eta_{\delta c}$ that are not known *a priori*. Three relations are needed to determine these unknowns. These relations are the matching of heat fluxes at the melt–condensate interface and the energy balance for each of these two layers. The matching of heat fluxes yields the interface temperature T_i as

$$\tilde{\theta}_m'(\tilde{\eta}_{\delta m}) = Pr_m^{1/4} R_3 \theta_c'(0)(T_f - T_i)/(T_i - T_{melt}) \tag{39}$$

where

$$R_3 = k_c c_c/(k_m c_m). \tag{40}$$

The energy balance at the melt front $y = 0$ or $\tilde{\eta}_m = 0$ is written as

$$k_m \partial T_m/\partial y|_{y=0} = \rho_m h_{sl} v_m|_{y=0}. \tag{41}$$

In terms of similarity variables equation (41) transforms to

$$c_{pm}(T_i - T_{melt})/(Pr_m h_{sl}) = -3\tilde{F}_m(\tilde{\eta}_m = 0)/\tilde{\theta}_m'(\tilde{\eta}_m = 0). \tag{42}$$

The energy balance at the free surface $y = \delta_m + \delta_c$, $\eta_c = \eta_{\delta c}$, or $\eta = 0$ can be written as

$$k_c \partial T_c/\partial y = k\partial T/\partial y - \rho_c h_{fg}[v_c - u_c \mathrm{d}(\delta_m + \delta_c)/\mathrm{d}x]. \tag{43}$$

Using the similarity variables equation (43) transforms to

$$c_{pc}(T_f - T_i)/h_{fg} = 3F_c(\eta_{\delta c})/\theta_c'(\eta_{\delta c}) + R_7 \varepsilon'(0)/\theta_c'(\eta_{\delta c}) \tag{44}$$

where

$$R_7 = kT_\infty c/(\rho_c h_{fg} \alpha_c c_c). \tag{45}$$

Condensation on a free liquid surface can be considered as an effusive molecular flow. In a real condensation process the net flow of vapor to the free surface will correspond to a drop in the temperature of the free surface or a lowering of the vapor pressure. The vapor pressure drop at the free surface is given in ref. [10] as

$$\Delta p = [q/(a h_{fg})][2\pi R_v T]^{1/2} \tag{46}$$

where R_v is the gas constant of the vapor. The vapor pressure drop at the free surface corresponds to a drop in the saturation temperature. Therefore this interfacial resistance will decrease the heat transfer rate at the melting wall.

Method of solution

For the purposes of computation it is advantageous to fix the temperature at the free surface, T_f, and then to determine what mass fraction of gas in the bulk, $m_{g\infty}$, corresponds to this temperature. Thus present calculations are made by parametrically varying T_f between T_{melt} and T_∞.

Upon inspection of the governing differential equations with the associated boundary and interface conditions it can be determined that if

$$F_c''(\eta_{\delta c}) = 0 \tag{47}$$

in equation (33) and

$$c_{pc}(T_f - T_i)/h_{fg} = 3F_c(\eta_{\delta c})/\theta_c'(\eta_{\delta c}) \tag{48}$$

in equation (44) then the condensate and melt layers are mathematically decoupled from the vapor–gas mixture layer. Equation (47) physically corresponds to the case of zero shear stress at the condensate layer free surface while equation (48) implies that the heat conducted to the free surface from the vapor–gas mixture is much less than the latent heat which is released upon condensation. Both of these conditions apply to the case of the condensate being steam with air mixed in it. For the cases examined here the exact calculations show that the assumption of zero shear stress results in an error in the wall heat transfer rate of less than 1% and the contribution of heat conduction to the free surface is less than 3% of the heat released by condensation. Therefore in the present analysis equations (47) and (48) replace the corresponding items in equations (33) and (44).

The equations governing the melt and condensate flows are mathematically coupled through their matching conditions at the melt–condensate interface. Inspection of the form of the differential equations and their boundary and interface conditions suggests that an easy solution algorithm can be developed if the melt and the condensate layers are uncoupled. This can be accomplished by assigning arbitrary values to the shear stress and the velocity at the melt–condensate interface. For assumed values of $Pr_m^{-1/4} R_2$, $Pr_m^{1/4} R_3$, Pr_m, Pr_c, $c_{pm}(T_f - T_{melt})/(Pr_m h_{sl})$, and $c_{pc}(T_f - T_{melt})/h_{fg}$ with condensate values evaluated at T_f the governing equations for the melt and the condensate are then numerically integrated while matching the boundary conditions at the free surface and at the wall. The corresponding melt and condensate parameters are then calculated from equations (42) and (48) and are compared to the assumed values. An iteration scheme is then used to find values

for the shear and the velocity at the melt–condensate interface that yield the assumed values of the melt and condensate parameters. Additional details are contained in ref. [2].

Having the results from the melt and the condensate layers, the vapor–gas layer is then analyzed. The mass fraction of the gas in the bulk, $m_{g\infty}$, is guessed. Knowing T_f, m_{gf} is calculated having the saturation pressure of the steam from the steam tables and the total pressure as well as the molecular weights of the air and the steam. The thermophysical properties of the vapor–gas mixture are calculated using mixture rules presented in ref. [11] with a reference mass fraction of the vapor equal to two-thirds of the free surface value plus one-third of the vapor mass fraction in the bulk. The reference temperature used is the sum of two-thirds of T_f and one-third of T_∞. At the free surface $f'(0)$, $f(0)$, $\varepsilon(0)$, $\phi(0)$, and $\phi'(0)$ are calculated using the known condensate values and equations (33). The values of $f''(0)$ and $\varepsilon'(0)$ are guessed and the vapor–gas mixture momentum, energy and species equations are numerically integrated from $\eta = 0$ to $\eta = \eta_{max}$. For the present applications η_{max} is less than 7. If at η_{max} the values of $f' \neq 0$ and $\varepsilon \neq 1$ then new guessed values for $f''(0)$ and $\varepsilon'(0)$ are used and the process is repeated. Finally if $\phi \neq 0$ at η_{max} a new guessed value for $m_{g\infty}$ is used and the whole process is repeated. Additional details of this method of solution are contained in ref. [12].

Using superscripts 0 and 1 to define the heat fluxes at the inner and outer edges of the films, respectively, the local Nusselt numbers for the melt and condensate layers can be written as

$$Nu_m^0 = \frac{x}{(T_i - T_{melt})} \left.\frac{\partial T_m}{\partial y}\right|_{y=0} = \gamma_m^0 \left[\frac{(\rho_m - \rho_\infty) g h_{sl} x^3}{4 \nu_m k_m (T_i - T_{melt})}\right]^{1/4} \quad (49)$$

$$Nu_c^1 = \frac{x}{(T_f - T_i)} \left.\frac{\partial T_c}{\partial y}\right|_{y=\delta_m+\delta_c} = \gamma_c^1 \left[\frac{(\rho_c - \rho_\infty) g h_{fg} x^3}{4 \nu_c k_c (T_f - T_i)}\right]^{1/4}. \quad (50)$$

If only the melting rate of the wall is to be determined a local Nusselt number based on the total temperature difference between the vapor–gas bulk and the melting surface can be defined as

$$Nu_t^0 \equiv \frac{x}{(T_\infty - T_{melt})} \left.\frac{\partial T_m}{\partial y}\right|_{y=0} = \gamma_t^0 \left[\frac{(\rho_m - \rho_\infty) g h_{sl} x^3}{4 \nu_m k_m (T_\infty - T_{melt})}\right]^{1/4}. \quad (51)$$

The Nusselt number based on the average heat transfer coefficient can be simply written as

$$\overline{Nu}_t^0 = \frac{4}{3} \gamma_t^0 \left[\frac{(\rho_m - \rho_\infty) g h_{sl} L^3}{4 \nu_m k_m (T_\infty - T_{melt})}\right]^{1/4}. \quad (52)$$

In the above equations γ_m^0, γ_c^1 and γ_t^0 are defined as

$$\gamma_m^0 = \left[\frac{c_{pm}(T_i - T_{melt})}{Pr_m h_{sl}}\right]^{1/4} \tilde{\theta}'_m(\tilde{\eta}_m = 0) \quad (53)$$

$$\gamma_c^1 = \left[\frac{c_{pc}(T_f - T_i)}{h_{fg}}\right]^{1/4} \theta'_c(\eta_c = \eta_{\delta c}) \quad (54)$$

$$\gamma_t^0 = \frac{(T_i - T_{melt})}{(T_\infty - T_{melt})} \left[\frac{c_{pm}(T_\infty - T_{melt})}{Pr_m h_{sl}}\right]^{1/4} \times \tilde{\theta}'_m(\tilde{\eta}_m = 0). \quad (55)$$

If a noncondensable gas is not present T_∞ and T_f are equal to the saturation temperature of the vapor, T_{sat}.

As mentioned earlier the interfacial resistance can be significant when the condensation rates are high. To consider the effect of interfacial resistance an average heat flux analysis is used. The average wall heat flux, q, is determined from equation (52). Knowing the average wall heat flux and the free surface temperature, the vapor pressure drop, Δp, at the free surface is determined from equation (46) with h_{fg} and T evaluated at the free surface temperature for no interfacial resistance. The new vapor pressure is equal to the pressure for no interfacial resistance minus Δp. This new value at the free surface is used to determine the saturation temperature and the average wall heat flux, q. This value of q is again used in equation (46) and the process is repeated until the calculated value of q equals the assumed value.

EXPERIMENTAL APPARATUS AND PROCEDURE

Simultaneous melting–condensation experiments were conducted by condensing steam with air mixed in it at a total pressure of 1 atm on the vertical faces of slabs of naphthalene and Wood's metal. In each run, data for the change in the mass of the slab were taken.

The apparatus used for performing experiments had essentially five components: a boiler to produce steam; an orifice plate to measure the steam flow rate; an airflow meter to measure and regulate the amount of air added to the steam; a viewing chamber in which the vertical slabs were placed; and a structure for holding the test slab in the viewing chamber. Figure 2 shows the experimental set-up.

Steam was produced in a boiler rated at 0.02 kg s^{-1} of saturated steam at 1 atm pressure. The part of the steam that is not bled off passes through a metering orifice plate. The differential pressure gauge around the orifice plate along with the upstream pressure gauge are used to determine the mass flow rate of the steam. The steam flow rate thus determined is accurate to within 5%. The steam temperature is measured with a thermocouple placed near the upstream pressure gauge. The mass flow rate of air is measured with a flow meter. The pressure and temperature of the air are measured with a pressure gauge and a thermo-

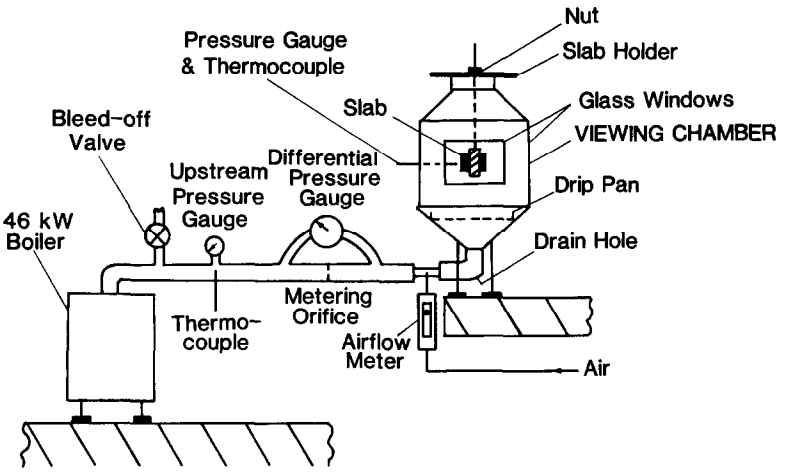

FIG. 2. Test apparatus.

couple placed at the outlet of the flow meter. With this arrangement the determined airflow rate is accurate to within 3%. The viewing chamber is made of 3-mm-thick stainless-steel sheet and has overall dimensions of $30 \times 30 \times 70$ cm. Glass windows are provided in two adjoining sides of the tank to facilitate visual observations of the melting–condensation process during the experiments. At the bottom of the viewing chamber is a 2-cm-diameter drain hole so that any water which condenses on the inner walls of the chamber is removed. The upper part of the viewing chamber is a truncated pyramid with a 15-cm-diameter opening at the top. The bottom part of the viewing chamber is also a truncated pyramid which joins a 2.5-cm-diameter elbow. The drain hole is drilled at the bottom of this elbow. Air is mixed with the steam in a short pipe attached to the elbow. The Reynolds number of the steam–air mixture within this pipe is calculated to lie in the turbulent range. Below the slab holder a 23-cm-diameter drip pan is placed in the lower pyramidal section. This drip pan not only catches the melt which drips from the test slab but also protects the slab from the blast of the steam–air jet exiting from the elbow. Thus the drip pan also acts as a deflection plate to obtain a near quiescent flow of the steam–air mix near the melting surface with a calculated velocity of less than 0.22 m s^{-1}. In the side of the viewing chamber near the location of the melting slab are placed a pressure gauge and a thermocouple to determine the pressure and temperature of the steam–air mix. The structure for holding the test slab is essentially a wooden frame the walls of which cover most of the four sides of the slab (top, bottom and the two sides) while allowing the front and the back an unobstructed exposure to the steam–air mixture. The frame is attached to a wooden bar through a threaded rod. During the experiments the slab holder with the test slab in it is suspended by placing the wooden bar over the top of the viewing chamber. The position of the suspended slab is adjusted by turning the nut on the threaded rod.

Prior to each experiment a slab of naphthalene or Wood's metal was cast. To make these slabs the test solid material was melted and poured into a wooden rectangular mold placed on an aluminum sheet which was wider than the width of the mold. The molten material was cooled from below by placing pieces of dry ice on the portions of the aluminum sheet extending out of the mold. This was necessary to initiate freezing at the bottom. A freezing front moving up from the bottom helped avoid cracking of the slab and yielded a smooth external surface. After casting, the slab was placed in a bath of warm water. The temperature of the bath was maintained 3 K below the melting temperature of the solid. This was done to make sure that almost all of the energy liberated during condensation was utilized only in melting of the solid. The steam flow rate to the viewing chamber was adjusted so that the energy content of the steam was several times the power needed for steady-state condensation–melting of the surface.

Experiments were conducted by securing the slab in the holder which was then lowered down the opening at the top of the viewing chamber. The experiments were terminated when the end effects or the changes in the shape of the melting surface were seen to begin to influence the melting rate.

After each experiment the test surface was visually examined. The visual observation showed uneven melting near the edges. To exclude the edge effects, the pits near the edges were filled with clay. Knowing the weight and the density of the clay the mass of the test solid needed to fill the pits was determined. This mass was then subtracted from the total mass lost by the slab during a particular experiment to determine the net melted mass, Δm, of the solid. The average heat transfer coefficient, $\bar{h}$, was then determined as

$$\bar{h} = \frac{\Delta m h_{sl}}{2(T_\infty - T_{melt}) W L \Delta t}. \tag{56}$$

In equation (56), W and L are the width and height of one test surface and Δt is the duration of the exper-

iment. It is shown in ref. [12] that the experimental values of $\bar{h}$ and γ_t^0 are accurate to within $\pm 11\%$ and $\pm 12\%$, respectively.

RESULTS AND DISCUSSION

In the absence of the noncondensables in the vapor, the values of γ_t^0 and the temperature drop across the melt or condensate layers can be obtained for large Prandtl number melts from ref. [1]. The results for low Prandtl number melts are shown in Figs. 3 and 4. Details of these results can be found in ref. [2]. In these two figures, the values of the dimensionless parameters are varied so that they cover the cases of uranium dioxide condensing on steel and steam condensing on Wood's metal. Figure 3 shows the dependence of the numerical constant γ_t^0 on the modified melt parameter $c_{pm}(T_{sat}-T_{melt})/(Pr_m h_{sl})$ while the condensate parameter $c_{pc}(T_{sat}-T_{melt})/h_{fg}$ and the melt Prandtl number are varied parametrically. The results for the two limiting cases of $Pr_m \to 0$ (no convective terms in the melt energy equation) and $c_{pc}(T_{sat}-T_{melt})/h_{fg}=0$ (melting alone) are also included in this figure. It is noted that for thicker melt layers, $\ln[c_{pm}(T_{sat}-T_{melt})/Pr_m h_{sl}] > 2$, the constant γ_t^0 depends strongly on the melt Prandtl number, hence convective terms in the melt energy equation cannot be neglected beyond this value of $c_{pm}(T_{sat}-T_{melt})/Pr_m h_{sl}$. The neglect of melt convective terms, in general, will result in overestimation of γ_t^0. For a given melt parameter the value of γ_t^0 decreases as the condensate layer becomes thicker or $c_{pc}(T_{sat}-T_{melt})/h_{fg}$ increases. It is seen that for the set of the dimensionless parameters used in this figure, the values of γ_t^0 are always below those for melting alone, $c_{pc}(T_{sat}-T_{melt})/h_{fg} \to 0$. Presence of a condensate layer affects the melt layer and the melting rate (or γ_t^0) in two ways. First, the condensate layer decreases the temperature drop across the melt layer which in turn causes reduction in the melting rate and γ_t^0. Second, the condensate layer enhances the heat transfer by introducing a positive shear at the melt surface (which results in a thinner melt layer). For the parameters used in plotting the results in Fig. 3, the increase in condensate layer thickness reduces the value of γ_t^0 for all $c_{pm}(T_{sat}-T_{melt})/Pr_m h_{sl}$. It is seen from Fig. 3 that as the melt parameter becomes large γ_t^0 does not depend strongly on the condensate parameter and the value of γ_t^0 approaches that for melting alone.

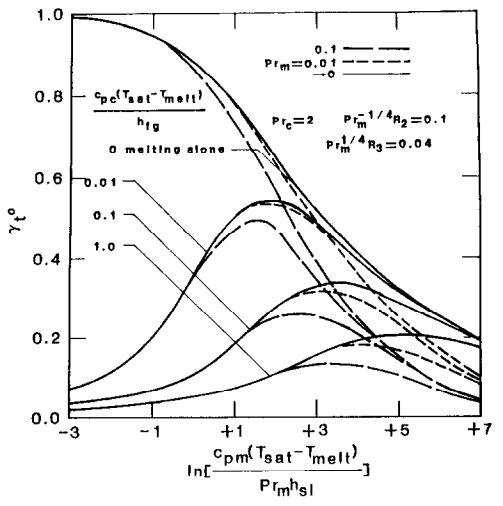

FIG. 3. Dependence of the constant γ_t^0 on $c_{pm}(T_{sat}-T_{melt})/Pr_m h_{sl}$ for different values of $c_{pc}(T_{sat}-T_{melt})/h_{fg}$ and Pr_m.

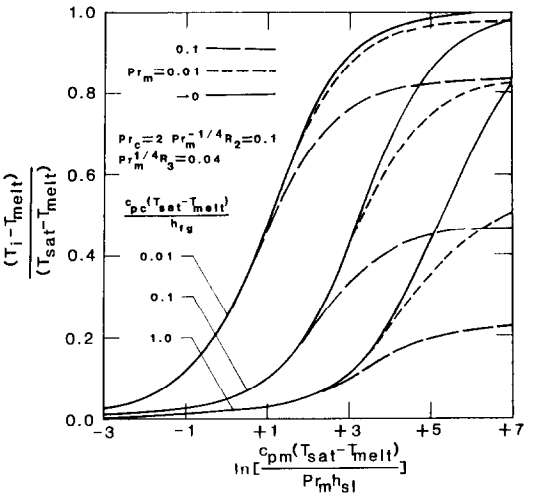

FIG. 4. Dependence of $(T_i-T_{melt})/(T_{sat}-T_{melt})$ on $c_{pm}(T_{sat}-T_{melt})/Pr_m h_{sl}$ for different values of $c_{pc}(T_{sat}-T_{melt})/h_{fg}$ and Pr_m.

The effect on γ_t^0 of varying the melt parameter is not as straightforward. The melt layer also affects the condensate layer in two ways. It reduces the shear at the inner surface of the condensate layer (melt–condensate interface) which results in a thinner condensate layer, hence higher heat transfer. It reduces the temperature drop across the condensate layer which causes a reduction in the heat transfer. For small values of the melt parameter, the enhancement in heat transfer resulting from the thinning of the condensate layer is more than the reduction caused by the decrease in the temperature drop across the condensate layer and as such γ_t^0 increases as the melt parameter is increased. However as the melt layer becomes thicker (where the shear at the melt–condensate interface is already small) the additional thermal resistance of the melt layer dominates any improvement in the heat transfer and values of γ_t^0 start to decrease.

Figure 4 shows the dependence of the ratio of melt-to-total temperature drop, $(T_i-T_{melt})/(T_{sat}-T_{melt})$, on the modified melt parameter, the condensate parameter and the melt Prandtl number. This ratio is seen to increase with increasing melt parameter (thicker melt layer) and with decreasing condensate parameter (thinner condensate layer). An interesting

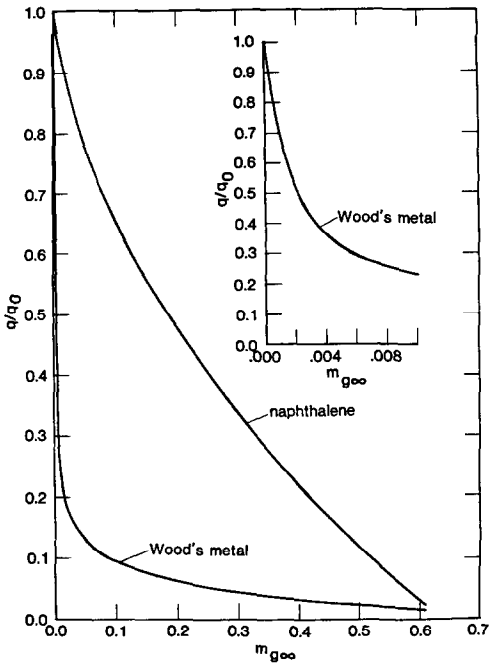

FIG. 5. Dependence of the ratio q/q_0 on $m_{g\infty}$ for naphthalene and Wood's metal slabs.

observation that can be made here is that for all cases $(T_i - T_{melt})/(T_{sat} - T_{melt})$ tends to approach an asymptotic value less than one as the melt layer becomes very thick, $c_{pm}(T_{sat} - T_{melt})/Pr_m h_{sl} \to \infty$. This behavior is expected since condensation has to occur to cause melting and hence some condensate film resistance will always be there.

The heat transfer to the wall can be calculated using equation (51) or (52) with γ_t^0 being the value for no gas in the vapor and T_∞ being the saturation temperature of the vapor.

In Fig. 5 are presented the analytical results of the heat flux at the wall with gas in the vapor, q, divided by the value q_0 with no gas. The results are plotted for steam with air in it at 1 atm total pressure and 100°C condensing on slabs of naphthalene and Wood's metal. Interfacial resistance is ignored in these figures. The insert is an enlarged graph for the Wood's metal case with mass fractions of the air varying from 0 to 0.01. As is apparent from the figure, non-condensable gas affects the heat transfer rate much more seriously for the case of Wood's metal than it does for the case of naphthalene.

To explain the above observation a simplified thermal model of the problem is developed as shown in Fig. 6. The thermal network consists of three resistances: that of the melt, the condensate, and the steam–air mixture. The steam–air mixture resistance, R, includes both the heat transfer by conduction from the mixture as well as the effect of resistance to vapor diffusion. If the resistance R is much less than the sum of the thermal resistances of the melt and the condensate, $(R_m + R_c)$, then to a very good approximation the thermal resistance of the mixture can be ignored. However, when R is of the order of $(R_m + R_c)$ or greater then the resistance of the vapor–gas mixture must be considered. Table 1 presents the analytical results for a 1 atm steam–air mixture at 100°C condensing on vertical surfaces of naphthalene and Wood's metal slabs. The slabs are assumed to have lengths and widths of 0.3048 m. A location at a distance of 0.0762 m (1/4 of the total length of the surface) from the leading edge is considered. The air mass fractions are 0.001 and 0.01. Interfacial resistance is ignored in this table. The thermal resistances are defined as

$$R_c + R = (T_\infty - T_i)/Q(y = \delta_m) \quad (57)$$

$$R_c = (T_f - T_i)/Q(y = \delta_m) \quad (58)$$

$$R_m = (T_i - T_{melt})/Q(y = \delta_m). \quad (59)$$

As is apparent from the table, a small mass fraction of gas has a negligible effect upon the heat transfer rate in the case of a naphthalene melt but does have a major effect when the melt is Wood's metal. This is because the Wood's metal melt, with its high thermal conductivity, has a very small thermal resistance. The naphthalene melt, with its lower thermal conductivity, has a larger resistance. Therefore the added thermal resistance of the mixture layer is insignificant for the case of naphthalene but is very significant in the case of Wood's metal.

In Fig. 7 are presented the analytical results of q/q_0 both without and with interfacial resistance for the case of a 1 atm total pressure steam–air mixture at 100°C condensing onto slabs of Wood's metal. The value q_0 is for the case of no interfacial resistance. The insert is an enlargement of the results for the range of $m_{g\infty}$ from 0 to 0.01. In calculating the interfacial resistance the value of the condensation coefficient a is taken to be 0.04. As can be observed from the figure, interfacial resistance does have a noticeable effect upon the wall heat transfer rate when a is 0.04 for the Wood's metal case. Results are not presented in graphical form for the case of naphthalene because the effect of interfacial resistance is very small. The reason for this is that the value of q_0 for naphthalene is less than 4% of that for Wood's metal. When a is assumed to be 1.0 the effect of interfacial resistance is

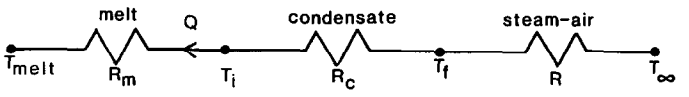

FIG. 6. Simple thermal network model of steam with air in it.

Table 1. Analytical results with no interfacial resistance for one atmosphere steam–air mix at 100°C condensing on vertical slabs at $x = 0.0762$ m

	Mass fraction of air			
	0.01		0.001	
	naphthalene–water	Wood's metal–water	naphthalene–water	Wood's metal–water
T_f (°C)	98.06	73.45	99.74	86.06
T_i (°C)	97.88	70.98	99.54	74.57
T_{melt} (°C)	80.00	70.00	80.00	70.0
$Q\|_{y=\delta_m}$ (W)	1.695×10^3	1.087×10^4	1.821×10^3	3.186×10^4
R (K W^{-1})	1.14×10^{-3}	2.44×10^{-3}	1.43×10^{-4}	4.38×10^{-4}
R_c (K W^{-1})	1.08×10^{-4}	2.27×10^{-4}	1.12×10^{-4}	3.61×10^{-4}
R_m (K W^{-1})	1.05×10^{-2}	9.03×10^{-5}	1.07×10^{-2}	1.44×10^{-4}
$R/(R_m + R_c)$	0.11	7.69	0.013	0.868
$q/q_0\|_{y=\delta_m}$	0.92	0.228	0.99	0.67

also very small for Wood's metal. It should also be mentioned that the present work's analysis for the condensate and melt layers includes the inertia and convective terms in the momentum and energy equations. If these terms were ignored the calculated wall heat transfer rates for Wood's metal and naphthalene would increase by about 22% and 7%, respectively.

The analytical results of steam with air in it condensing onto naphthalene and Wood's metal slabs are presented in this paper. If other large and small Prandtl number melts are considered, as an engineering approximation the value of q can be estimated from Fig. 5 using the curve for naphthalene to approximate large Prandtl number melts and the Wood's metal curve to approximate small Prandtl number melts. If accurate wall heat transfer rates are required the computer code presented in ref. [12] should be used.

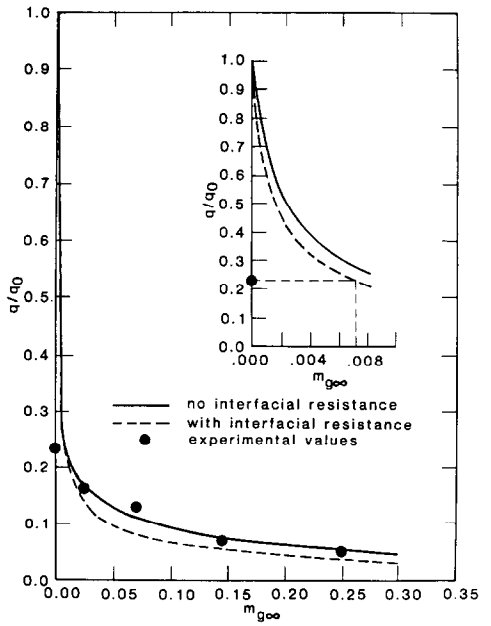

FIG. 7. Comparison of the Wood's metal data with analytical results. Condensation coefficient $a = 0.04$.

Several experiments were conducted by condensing steam with air in it at 1 atm total pressure onto slabs made of naphthalene and Wood's metal. The thermophysical properties of these materials are listed in ref. [2]. The vertical surfaces were generally 10 cm high and 7.7 cm wide. The experiments lasted about 1 min. The duration of the experiments was chosen so that the end effects remained small and no appreciable change in the shape of the surface occurred. Using the results presented in ref. [13], it is found that the small change in the shape of the initially vertical surface during the experiments would have amounted to about a 3% change in the melting rate. However the time periods of the experiments were much longer than the times needed for the melt and condensate layers and the solid melt to attain their steady states. Using the analysis presented in ref. [9] the maximum steady-state times for the melt and condensate layers in the naphthalene and Wood's metal experiments were 2.71 and 1.18 s, respectively. The melting process will initially also be unsteady due to the subcooling of the slabs. For a subcooling of about 3°C, which was typical of the slabs used in the experiments, the time for the process to reach steady state is calculated from ref. [8] to be less than 1 s.

It is shown in ref. [12] that for a distance 1.5×10^{-5} m from the leading edge, the increased pressure due to surface tension and curvature of the interface will be less than 1% of the system pressure of 1 atm. Visual observations of the melting–condensation process showed that the vapor condensed in the form of a film and both the melt and condensate films flowed downwards. The water film was seen to be free of any ripples. The maximum Reynolds numbers for the melt and condensate films are calculated to be less than 750, thus both films are expected to be laminar. On post-experiment examination the vertical surface was found to be generally flat with the upper horizontal edge and the vertical edges slightly contoured. The contouring of the upper horizontal edge was caused by faster melting at the leading edge while that at the sides was caused by exposure to the vapor on the two sides.

The experimental values of γ_t^0 and $\bar{h}$ which are

Table 2. Comparison of the predicted (both without and with interfacial resistance) and the observed values of the coefficient γ_t^0 and the average heat transfer coefficient $\bar{h}$. Condensation coefficient $a = 0.04$

	Melt–condensate								
	Naphthalene–water				Wood's metal–water				
$m_{g\infty}$	0.000	0.195	0.198	0.198	0.000	0.025	0.070	0.145	0.250
Surface height L (m)	0.098	0.092	0.095	0.096	0.100	0.100	0.100	0.100	0.100
Surface width W (m)	0.075	0.070	0.072	0.073	0.076	0.077	0.077	0.076	0.077
Duration of experiment Δt (s)	43.3	67.5	65.4	69.4	13.2	38.7	55.7	67.6	54.2
Temperature of mixture T_∞ (K)	371	367	368	368	372	373	372	370	368
Predicted γ_t^0 no resistance	0.945	0.471	0.466	0.466	0.320	0.055	0.036	0.026	0.017
Predicted $\bar{h}$ no resistance (kW m^{-2} K^{-1})	1.09	0.547	0.541	0.540	20.8	3.55	2.32	1.68	1.11
Predicted γ_t^0 with resistance	0.943	0.469	0.464	0.464	0.308	0.043	0.027	0.019	0.012
Predicted $\bar{h}$ with resistance (kW m^{-2} K^{-1})	1.09	0.545	0.539	0.538	20.0	2.81	1.76	1.22	0.774
Data γ_t^0	0.857	0.543	0.518	0.546	0.075	0.053	0.041	0.024	0.016
Data $\bar{h}$ (kW m^{-2} K^{-1})	0.988	0.631	0.601	0.633	4.85	3.45	2.68	1.56	1.03
% Error no resistance	−9.3	+15.3	+11.3	+17.2	−76.7	−2.9	+15.3	−7.1	−7.2
% Error with resistance	−9.1	+15.8	+11.6	+17.7	−75.8	+22.8	+51.8	+27.7	+33.3

determined by knowing the net melted mass lost during the experiment and using equations (52) and (56) are listed in Table 2. In this table the analytical values of γ_t^0 and $\bar{h}$ are also included both without and with interfacial resistance with $a = 0.04$. The analysis assumes that the bulk temperature of the steam–air mixture is 373 K. The change in the total heat flux at the free surface is less than 1% when it is assumed that the bulk temperature is 373 K rather than the actual experimental mixture temperature. The experimental and analytical naphthalene wall heat transfer values are within 18% of each other. Experimental values for the case of Wood's metal are also presented in Fig. 7. The data values hug the analytical curve for no interfacial resistance but are slightly above the curve which accounts for the interfacial resistance with a condensation coefficient of 0.04. It is noted that with the exception of the data point for $m_{g\infty} = 0$ (pure vapor), the observed values of γ_t^0 lie within +15% and −7% of the no interfacial resistance predictions and those with $a = 1.0$. However, the experimental values are up to 52% higher than the analytical values which include interfacial resistance with $a = 0.04$.

The reason why the experimental value for Wood's metal at $m_{g\infty} = 0$ is much less than the analytical value can be explained with the use of Table 1. Whereas a small amount of air will not affect the naphthalene results significantly the opposite is true for the Wood's metal case. It is impossible to eliminate all of the air from the experimental set-up. There will always be some air trapped in the feed-water to the boiler, within the slabs themselves during casting, etc. It is seen from Fig. 7 that the environment which was considered to be free of noncondensables actually could have had up to about 0.76% mass fraction of air in it. In the other experiments in which air was deliberately introduced into the chamber, the added amount of air overwhelmed this small amount of resident air making the amount of air initially present insignificant.

CONCLUSIONS

1. Similar solutions can be obtained to the full boundary-layer equations which govern the simultaneous melting–condensation of a three-component system with a noncondensable gas present in the vapor provided interfacial resistance is ignored.
2. The analytical results of simultaneous melting–condensation on vertical walls with air present in the steam show that the air affects the wall heat transfer rate much more severely for the low Prandtl number Wood's metal melt than it does for the high Prandtl number naphthalene melt.
3. Interfacial molecular resistance is much more significant in the case of a liquid metal melt layer than it is for a large Prandtl number melt.
4. The experiments conducted by condensing steam with air in it at a total pressure of one atmosphere on vertical surfaces of naphthalene slabs show that the observed melting rates compare within +18% and −9% of the predicted values. For Wood's metal slabs with the exception of the no added air experiment the observed values were within +15% and −7% of the predictions based on no interfacial resistance and those with interfacial resistance but $a = 1.0$. The analysis which assumed interfacial resistance with a condensation coefficient of 0.04 showed that the experimental values were consistently higher with the exception of the $m_{g\infty} = 0$ experiment.

5. The very low value observed in the experiment with Wood's metal in which $m_{g\infty} = 0$ is attributed to the experimental difficulty in completely eliminating the noncondensable air from the system.

REFERENCES

1. K. Taghavi-Tafreshi and V. K. Dhir, Analytical and experimental investigation of simultaneous melting–condensation on a vertical wall, *J. Heat Transfer* **104,** 24–33 (1982).
2. K. Taghavi-Tafreshi, Condensation of saturated vapor on melting surfaces. Ph.D. dissertation, UCLA, Los Angeles, CA (1982).
3. E. M. Sparrow and S. H. Lin, Condensation heat transfer in the presence of a noncondensable gas, *J. Heat Transfer* **86,** 430–436 (1964).
4. W. J. Minkowycz and E. M. Sparrow, Condensation heat transfer in the presence of noncondensables, interfacial resistance, superheating, variable properties, and diffusion, *Int. J. Heat Mass Transfer* **9,** 1125–1144 (1966).
5. Y. C. Yen, A. Zehnder, S. Zavoluk and C. Tien, Condensation–melting heat transfer in the presence of air, *A.I.Ch.E. Symp. Ser.* **69,** 23–29 (1972).
6. D. F. Othmer, The condensation of steam, *Ind. Engng Chem.* **21,** 577–583 (1929).
7. C. Tien and Y. C. Yen, Condensation–melting heat transfer, *Chem. Engng Prog. Symp. Ser.* **67,** 1–9 (1971).
8. H. G. Landau, Heat conduction in a melting solid, *Q. appl. Math.* **8,** 81–94 (1950).
9. D. Galamba and V. K. Dhir, Transient simultaneous condensation and melting of a vertical surface, *J. Heat Transfer* **107,** 812–818 (1985).
10. Y. Y. Hsu and R. Graham, *Transport Processes in Boiling and Two-phase Systems*, p. 57. Hemisphere, Washington, DC (1976).
11. D. K. Edwards, V. E. Denny and A. F. Mills, *Transfer Processes*, 1st edn, p. 206. Hemisphere, Washington, DC (1976).
12. D. Galamba, Some aspects of simultaneous melting–condensation of vertical surfaces. Ph.D. dissertation, UCLA, Los Angeles, CA (1986).
13. K. Taghavi-Tafreshi and V. K. Dhir, Shape change of an initially vertical wall undergoing condensation-driven melting, *J. Heat Transfer* **105,** 235–240 (1983).

ETUDE ANALYTIQUE ET EXPERIMENTALE DE FUSION ET CONDENSATION SIMULTANEES SUR UNE PAROI VERTICALE EN PRESENCE D'UN GAZ INCONDENSABLE

Résumé—On étudie analytiquement et expérimentalement la fusion et la condensation simultanées sur une paroi verticale avec gaz incondensable dans la vapeur. En utilisant des transformations de similitude, les équations de couche limite gouvernant le bain non miscible, les couches de condensat et de vapeur–gaz sont résolues numériquement. Des résultats sont obtenus pour le flux thermique de fusion avec ou non une résistance interfaciale. Dans l'analyse on considère le nombre de Prandtl du bain faible ou élevé tandis que le condensat est supposé être un liquide à nombre de Prandtl élevé. Des expériences sont conduites avec de la vapeur d'eau, contenant de l'air, qui se condense sur des surfaces verticales de naphtalène et sur des plaques de métal de Wood. Les résultats expérimentaux se comparent bien avec les prévisions faites dans le cas sans résistance interfaciale et du grand coefficient de condensation.

ANALYTISCHE UND EXPERIMENTELLE UNTERSUCHUNG VON GLEICHZEITIGEM SCHMELZEN UND KONDENSIEREN AN EINER SENKRECHTEN WAND IN ANWESENHEIT VON NICHTKONDENSIERENDEM GAS

Zusammenfassung—Gleichzeitiges Schmelzen und Kondensieren an einer senkechten Wand mit nichtkondensierbarem Gas im Dampf wird analytisch und experimentell untersucht. Mit Ähnlichkeitstransformationen werden die vollständigen Grenzschichtgleichungen, die die nichtmischbare Schmelze, das Kondensat und die Dampf-Gas-Schichten beschreiben, numerisch gelöst. Ergebnisse für die Wärmeübertragung beim Schmelzen mit oder ohne nichtkondensierbare Gase und mit Grenzflächenwiderstand werden ermittelt. In der Untersuchung werden Schmelzen mit niedrigen und hohen Prandtl-Zahlen betrachtet, während das Kondensat als Fluid mit hoher Prandtl-Zahl angenommen wird. Experimente werden mit lufthaltigem Dampf,. welcher an senkrechten Naphthalin-Oberflächen und Wood's-Metallplatten kondensiert, durchgeführt. Die Ergebnisse stimmen gut mit den Berechnungen ohne Grenzflächenwiderstand und hohen Wärmeübergangskoeffizienten bei der Kondensation überein.

АНАЛИТИЧЕСКОЕ И ЭКСПЕРИМЕНТАЛЬНОЕ ИЗУЧЕНИЕ ПРОТЕКАЮЩИХ ОДНОВРЕМЕННО ПРОЦЕССОВ ПЛАВЛЕНИЯ И КОНДЕНСАЦИИ НА ВЕРТИКАЛЬНОЙ СТЕНКЕ В ПРИСУТСТВИИ НЕСЖИМАЕМОГО ГАЗА

Аннотация—Аналитически и экспериментально исследуются одновременные процессы плавления и конденсации на вертикальной стенке при наличии смеси несжимаемый газ-пар. Используя преобразования подобия, численно решена система уравнений пограничного слоя для несмешивающихся слоев расплава, конденсата и парогазовой смеси. Получены результаты для интенсивности теплопереноса при плавлении как в присутствии, так и в отсутствие неконденсирующихся газов и сопротивления на межфазной границе. Рассматриваются расплавы с малыми числами Прандтля, в то время как конденсат является жидкостью с большим числом Прандтля. Проведены эксперименты по конденсации смеси пар-воздух на вертикальных поверхностях нафталиновых слитках и слитках из сплава Вуда. Найдено хорошее соответствие экспериментальных данных и резулвтатов, полученных в отсутствие межфазного сопротивления и в предположении высоких значений коэффициента конденсации.